ELSEVIER

Contents lists available at ScienceDirect

# Bioelectrochemistry

journal homepage: www.elsevier.com/locate/bioelechem



# Flow micropillar array electroporation to enhance size specific transfection to a large population of cells



Yingbo Zu<sup>a,b,1</sup>, Xuan Liu<sup>c,d,1</sup>, An-Yi Chang<sup>a,b,d</sup>, Shengnian Wang<sup>a,b,c,d,\*</sup>

- <sup>a</sup> Chemical Engineering, Louisiana Tech University, PO Box 10137, Ruston, LA 71272, USA
- <sup>b</sup> Institute for Micromanufacturing, Louisiana Tech University, PO Box 10137, Ruston, LA 71272, USA
- <sup>c</sup> Macromolecular and Nanotechnology, Louisiana Tech University, PO Box 10137, Ruston, LA 71272, USA
- d Center for Biomedical Engineering and Rehabilitations, Louisiana Tech University, PO Box 10137, Ruston, LA 71272, USA

#### ARTICLE INFO

#### Article history: Received 9 July 2019 Received in revised form 14 November 2019 Accepted 17 November 2019 Available online 4 December 2019

Keywords:
Electroporation
Micropillar array
Carbon electrode
Transfection enhancement
Nonviral transfection

#### ABSTRACT

Despite serving as a popular non-viral delivery approach, electroporation carries several drawbacks in its current configurations. We developed a Flow Micropillar-array Electroporation (FME) system to wisely regulate an important transmembrane-determining factor, namely cell size variations among individual cells, to achieve effective transfection. In FME, cells flow through a slit-type microfluidic channel on which carbon electrodes with well-patterned micropillar array texture are integrated as the top and bottom wall. Gravity helps bring cells to the micropillar array surface so that the permeable area on cells in different size populations is specified by their size regardless their random location fact. Without sacrificing cell viability, we demonstrate this FME concept by delivering DNA plasmids to several mammalian cell lines with obvious transfection enhancement when compared to a commercial system (K562: 3.0 folds; A549: 3.3 folds; HeLa: 1.8 folds, COS7: 1.7 folds; 293T: 2.9 folds; mES: 2.5 folds). Moreover, carbon-based electrodes are less expensive, more durable, and convenient for integration with a microfluidic setup which enables rapid and massive transfection capability that many therapeutic application needs. The success of FME may benefit many emerging biological studies and clinical practice that requires effective transfection to a large population of cells in limited processing time.

© 2019 Published by Elsevier B.V.

#### 1. Introduction

Electroporation works using short, high-voltage electric pulses to surpass the plasma membrane capacitance of subjected cells to make it transiently permeable to exogenous cargos [1]. Owing to its balance of operation simplicity, transfection effectiveness, and broad allowance on probe or cell types, electroporation is quickly adopted in the past two decades in many biological and medical studies to deliver molecular medicine (e.g., plasmid DNA, oligonucleotides, and molecule drugs) into cells or tissues [2,3]. It serves as a prominent tool to understand gene functions [4], control cellular signals [5], and apply in cell-based therapeutic trials [6]. Among these applications, single cell electroporation (SCE) focuses on the discovery of cellular transport dynamics and mechanism (i.e., electrophysiology) [7–10] while bulk electroporation (BE) devotes in high transfection efficiency to cells of a large

population [1–3,11–13]. Although SCE findings could offer some guidance on cell electroporation conditions (e.g., electric field, electroporation medium, cell size and orientation), protocols of BE (i.e., pulse amplitude, duration, and number) are still established by trial-and-error in most situations, as a compromise of transfection efficiency and cell viability due to the heterogeneity of treated cells (cell type, source, population, and membrane permeability), local field conditions, and multiple side effects associated with the applied high-voltage pulses (e.g., Joule heating, electrochemical reactions in medium and composition of electrode) [14–16].

Several new electroporation setups with micro-/nanoscale features have been introduced in the past two decades, focusing on eliminating the aforementioned electroporation induced toxicity issues, either through closely patterning electrode pairs (e.g., ~20  $\mu m$ ) [17–25] and/or with micro/nanofluidic channel constriction [26–40]. These microelectroporation systems also offer new advantages over the commercial systems, namely *in situ* monitoring of intracellular content transport and electroporation dynamics at single cell level [41–43], better accuracy, and more flexibility on treatment in different cell populations [30–40]. However, most of these microelectroporation systems still ignore the variations

<sup>\*</sup> Corresponding author at: Chemical Engineering, Louisiana Tech University, PO Box 10137, Ruston, LA 71272, USA.

E-mail address: swang@latech.edu (S. Wang).

<sup>&</sup>lt;sup>1</sup> These authors contribute equally.

among individual cells in a large population such as the size and electrical properties differences of the treated cells, leaving many transmembrane-determining factors yet uncontrolled just like in commercial systems. Recently, we invented a simple but effective platform, micropillar array electroporation operated in batch mode (designated as "BME"), to accomplish cell size specific electroporation to cells [44]. In this BME system, cells are sandwiched between two parallel plate electrodes with one of them carrying a large array of well-patterned micropillars on its surface. When cells approach to the electrode, the number of micropillars each cell faces varies with its membrane surface area or the size of cells so that the pore formation is independent of the random dispersion status of cells as micropillars form a regular array on the electrode surface, as shown in Fig. 1. This makes it work like many SCE units are carried out in parallel with no need for cell positioning. We have successfully demonstrated the feasibility of this new cell size specific electroporation platform on plasmid and oligonucleotides delivery on different mammalian cell lines. However, two major limitations of this BME platform impede its broad acceptance in cell therapy practice. The first one comes from its batch operation format, which allows a cell processing speed similar to what in the commercial cuvette-based systems. For some emerging transfection explorations such as drug screening [45,46], cancer immune therapy [47], and cell reprogramming [48], rapid, effective transfection of healthy copies of DNA or RNA probes to a cell population of 10<sup>8</sup>–10<sup>9</sup> is often required. To meet such needs on massive transfection, we developed a new Flow Micropillar array Electroporation (FME) platform, in which a flow-through operation mode is configured with a micropillar array electrode integrated as the wall surface of a millimeter wide, micrometer deep flow slit. In this way, the same cell size specific electroporation to a large population of cells could be carried out in high throughput. The second limitation of previous BME platform lies on its gold-coated micropillar array electrode. Besides its high cost, the thin, precious metal layer could be gradually worn out from the polymer base of its micropillar array electrode when high current spikes passed periodically. Unlike batch operation mode, continuously flow operation of electroporation demands frequent pulse application schemes. This requires electrodes with steady electrical properties so that many pulses of the same voltage profile can be imposed on cells that pass the electroporation zone in microflow. To ensure similar cell size specific treatment as in BME, we directly convert the original SU-8 based micropillar array into conductive glassy carbon electrode through a carbon-MEMS based pyrolysis process. The received carbon micropillar array electrode is then integrated onto the microfluidic platform which also serves as its side wall. We evaluate this new FME system on plasmid DNA delivery to several adherent and suspension cell lines. Comparisons were made between these two different cell size-specific electroporation systems (BME vs FME) to find out how the two new features (i.e., microfluidic operation and carbon-based electrodes) in FME benefit the transfection effectiveness and cell survival situation.

#### 2. Experimental methods

#### 2.1. Materials and reagents

Gold target for sputter instrument was purchased from Ted Pella Inc. Pt sheet was purchased from Surepure Chemicals Inc. SU-8 5 photoresist (photosensitive polymer used for microfabrication) was purchased from Microchem, Inc. DNA plasmids with pMaxGFP reporter genes were purchased from Lonza, Inc. All other cell culture reagents were purchased from Life Technologies (Carlsbad, CA) unless specified.

#### 2.2. Cell culture

K562 cells (ATCC, CCL-243), A549 (ATCC, CCL-185), HeLa (ATCC, CCL-2), COS-7 (ATCC, CRL-1651), and 293 T (ATCC, CRL-3216) were cultured in RPMI 1640 supplemented with 10% newborn calf serum (NCS), 100 U/mL penicillin, 100 μg/mL streptomycin, and 100 μg/mL L-glutamine. Mouse embryonic stem (ATCC, CRL-1934) were cultured on gelatin-coated tissue culture flasks and maintained in an undifferentiated state using Dulbecco's Modified Eagle's Medium (DMEM with 4.5 g/l D-glucose) supplemented with 15%(v/v) fetal bovine serum (FBS), 100 U/ml penicillin, 100 μg/ml streptomycin, 0.1 mM non-essential amino acids, 10 ng/ml murine recombinant leukemia inhibitory factor (LIF), 0.1 mM monothioglycerol, 2 mM L-glutamine (Sigma Aldrich, St. Louis, MO) and 1 mM sodium pyruvate (Invitrogen). All cultures were maintained at 37° C with 5% CO<sub>2</sub> and 100% relative humidity.

#### 2.3. Carbon micropillar array electrode fabrication

Micropillar arrays were fabricated by BioMEMS technologies. Briefly, two layers of SU-8 5 photoresist (PR) were patterned on a Si (1 0 0) wafer via photolithography, as shown in Fig. 2a. The bottom PR layer was baked and floor exposed prior to application of the second layer of SU 8 PR. This SU-8 layer later serves as the conductive carbon base of the micropillar electrode. Micropillars (2 μm in diameter and 2 μm in height) were defined in a 2.54 m  $m \times 2.54$  mm square region on the top SU-8 layer with a pitch size of 4 µm (Fig. 2b). The produced SU-8 micropillars were further converted into glass carbon like conductive electrode in a quartz tube furnace under N2 gas. Three major steps were involved in this pyrolysis-based carbon electrode fabrication process: (i) thermal stabilization step; a wafer carrying SU-8 micropattern was heated from room temperature to 200 °C at 5 °C/min, followed by a 30 min dwell in an open air environment to remove solvent and thermally stabilize the micropillar structure; (ii) carbonization; SU-8 micropillars were then heated to 900 °C with a guick temperature ramp speed of 15 °C/min and further one hour dwell at the same temperature in N<sub>2</sub> gas flow to convert SU-8 micropattern to carbon based one; and (iii) annealing; carbon micropillar pattern was then cooled down to room temperature at a cooling rate of 5 °C/min in N<sub>2</sub> flow to release the stress built in carbon micropillars due to the mass loss and dimension shrinkage during the carbonization step. The complete carbonization procedure is presented in Fig. 2c and the finished carbon micropillar array pattern was shown in Fig. 2d.

# 2.4. Flow-through micropillar array electroporation (FME) platform assembly

To integrate the carbon micropillar array electrode on a microfluidic device, a pair of polymethylmethacrylate (PMMA) blocks was first machined to have an electrode holder and two shallow flow channels or tube connection ports, as shown in Schematic 1. A piece of carbon micropillar array electrode and a plain ITO-coated glass electrode were then fixed to the electrode holder on one PMMA block by adhesive glue, respectively. A PDMS gasket (~160 μm high) with a straight channel in the middle was then placed on top of the carbon micropillar array electrode to provide the slit-type flow space in FME after assembly. It also protects those micropillars during the next assembly step. After placing the second PMMA block (having the ITO electrode) facing down on top of the first PMMA block with carbon micropillar electrode, the three pieces (two PMMA blocks and one PDMS gasket) were clapped together to seal the flow channel. Plastic tubes were further mounted in the flow ports of PMMA blocks on both sides to complete the assembly. After the microfluidic device was exposed under UV light overnight, cleaned with 70% alcohol successively,

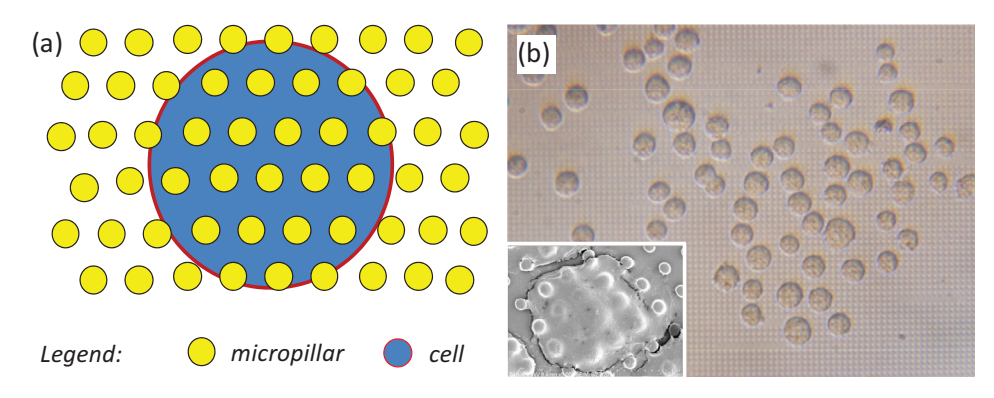


Fig. 1. The working principle of the micropillar array electroporation. (a) Schematic of the cell size-specific treatment mechanism (large cells face more micropillars with each providing focused electric pulse during electroporation); (b) an optical microscopy photo and a SEM image (inset) of K562 cell settlement on 2-µm micropillar array.

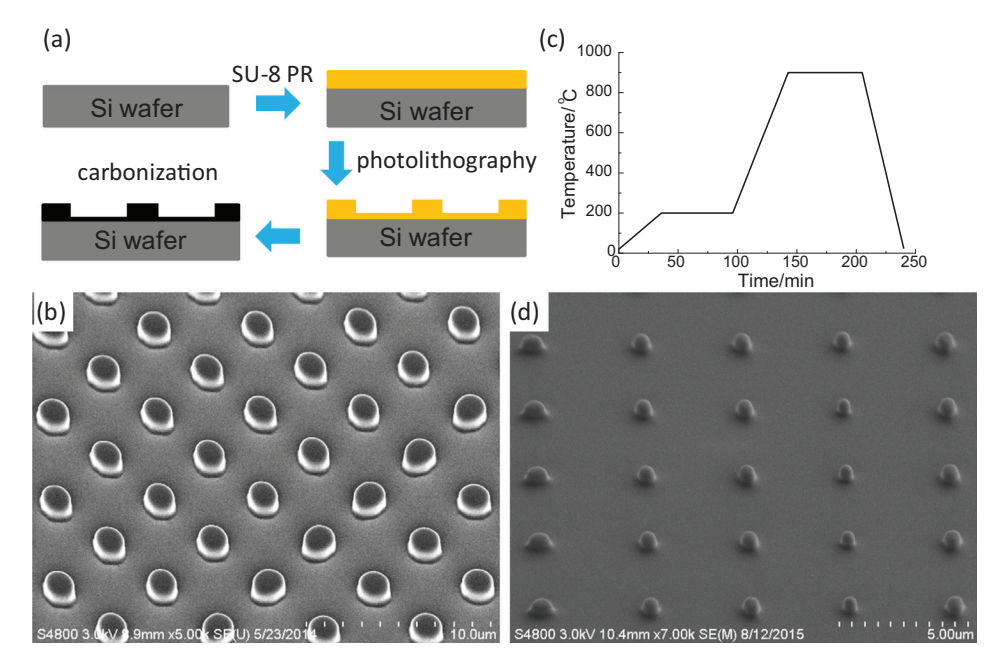


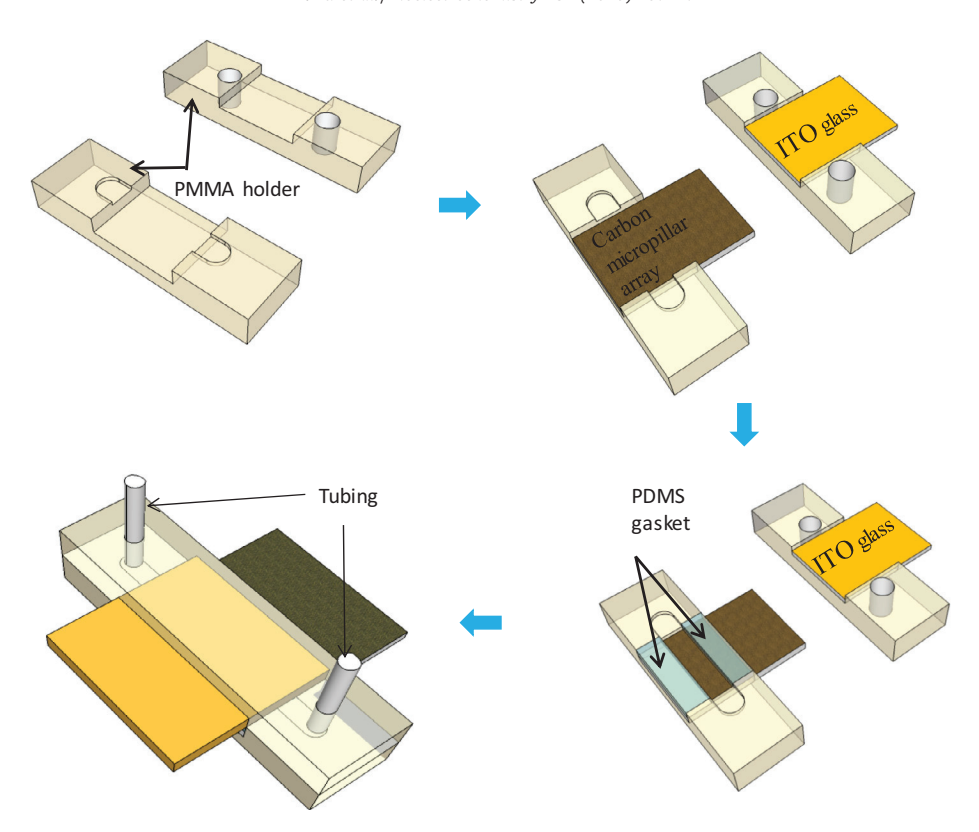
Fig. 2. Fabrication of carbon micropillar electrode by carbon MEMS technology. (a) schematic illustration of micropillar array fabrication by photolithography with SU-8 photoresist; (c) the carbonization temperature profile used for converting SU-8 micropillars to carbon micropillars; SEM images of micropillar array made of SU-8 (b) and carbon (d).

and extensively rinsed with phosphate-buffered saline (PBS), a slittype flow channel of 160  $\mu m$  high, 1 mm wide, and a 2.54 mm long was ready for cell loading, electroporation, and collection. Prior to electroporation, copper wires were bonded to the protrusive part of the two electrodes on PMMA block, which were further connected to a commercial pulse generator system (BTX ECM 830, Harvard Apparatus).

# 2.5. FME electroporation setup and operation procedure

Cells were first centrifuged and re-suspended in fresh OPTI-MEM I (a serum free medium) at a density of  $0.5 \times 10^7$  cells/ml. Plasmid DNA (i.e., pmaxGFP plasmids) of 10  $\mu$ g was then added to make the electroporation sample solution of 100  $\mu$ l. After prerinsing with opti-MEM medium, cell samples are loaded in the FME flow channel. Prior to sample loading, samples are gently mixed with a pipette to ensure cells are in individual suspension state or as small clusters to avoid potential channel clogging while achieve effective contact with micropillars for best size-specific treatment. Electric pulses of 10 V (with 10-ms pulse duration and one pulse per second) are then continuously imposed when

the cell solution is pumped through the FME channel at a flow rate of 1.5 ml/hr controlled by a programmable syringe pump (Pump 22, Harvard Apparatus, Holliston, MA). Cell samples flow through the FME channel at this pre-specified flow rate so that every cell experience single 10-ms pulse like what happens in the commercial systems for comparison. After electroporation, the channel was washed with opti-MEM I medium at a flow rate of 5 ml/hr to ensure most porated cells were cleaned out. After triple the amount of opti-MEM I medium for electroporation is pumped through the channel, another fresh cell solution sample is loaded into the FME channel to get ready for next electroporation. In each FME electroporation run, a 100-µl cell solution was pumped into the FME channel, the same amount that is also used in a 2-mm cuvette of a batch-mode commercial system (Bulk Electroporation, or BE). As the proof of concept, single microfluidic slit is used to process the same number of cells as in standard electroporation. About 270 pulses in total are applied to complete each 100 µl cell solution. Extra pulses (~30 pulses in 30 s) were given during the pre-loading and afterwards washing time to ensure all loaded cells receive electroporation. After treatment, cells were transferred to 6-well plates and cultured for another 24 hr before analysis. For



Schematic 1. Illustration of flow micropillar-array electroporation (FME) device assembly process.

comparison, standard electroporation was also done using the same BTX ECM 830 pulse system. Samples of 100  $\mu l$  each were first flown through the same FME channel without pulse application to avoid possible cell loss in microfluidic setup or cell number difference between flow and batch electroporation samples. Those samples were collected and loaded into standard electroporation cuvettes with two parallel electrodes separated by 2 mm and an optimal electroporation protocol (125 V, single 10-ms pulse) was applied.

# 2.6. Transfection efficiency and cell viability

The expression of pmaxGFP plasmids was evaluated both qualitatively by visualizing cells with green fluorescence within some representative areas under an inverted fluorescence microscope (Olympus, Japan) and quantitatively by counting cells using an Agilent 2100 Bioanalyzer (Agilent Technologies, Santa Clara, CA). The fluorescence intensity of GFP was measured using the Cell Assay Module with live cells stained with carboxy-naphthofluorescein (CBNF). The results were analyzed with Agilent 2100 Expert Software and 500-1500 events were counted for each sample. The transfection efficiency was also measured by a flow cytometry (CytoFLEX, Beckman Coulter), which was further used to check the potential impact of FME on cell morphology and its broad effectiveness on plasmid transfection to cells of different size populations simultaneously. At least 10,000 events were collected for each sample in flow cytometry measurement. Two types of control samples were included like what are done in other electroporation work [49]: one for cell viability analysis and one for autofluorescence assessment. For control I samples, cells and plasmid mixtures were flown through FME channel without applying electric pulses. They were used to normalize the cell viability signal for each electroporation samples. Control II samples were prepared under the same conditions as those for experimental cells, except

that no plasmid was added to the electroporation buffer solution. They were used to exclude debris and gate forward (FSC) and side (SSC) light scatter signals to isolate the live cell population only. CytExpert software was used for all data analysis. The transfection efficiency of pmaxGFP is defined as the percentage of cells emitting green fluorescence signal among all counted cells in a sample (gated fluorescence signal of GFP).

The cell viability was evaluated by an MTS assay (Promega. Madison, WI), in which the NAD(P)H-dependent dehydrogenase enzymes in metabolically active cells cause the reduction of MTS tetrazolium compound and produce colored formazan product that is soluble in cell culture media. Given our new electroporation technology targets cell therapeutic applications, this proliferation-based cell viability evaluation is critical to reveal the potential disturbance of electric pulses on cell metabolic activity. In MTS assay, 100 µl cells from each sample 24 hr post electroporation were harvested from a 6-well plate and transferred to a 96-well plate. CellTiter 96 AQueous One solution (Promega, Madison, WI) of 20 µl was added to each well and all samples were incubated at 37 °C for another 4 hr. Absorbance was measured at 492 nm on an automated plate reader (Elx 800, Biotek, VT). The cell viability is calculated as the absorbance signal ratio of an electroporated cell sample to that of the negative control cell sample (control I) in MTS assay, after extracting the absorbance background from the media. Data points were represented as the mean ± standard deviation (SD) of triplicates, unless otherwise indicated.

# 2.7. SEM sample preparation

A drop of cell solution was first applied on the micropillar electrode surface. Cells were then fixed with 2% glutaraldehyde in PBS buffer, followed by dehydration in a series of ethanol solutions with increasing concentration between 25 and 100% (25%/step,

20 min immersion in each step). The sample in 100% ethanol was further dried with  $CO_2$  in a critical point drier to preserve the cell morphology. All scanning electron microscope (SEM) micrographs were acquired using a Hitachi 4800 SEM (operating voltage 1.0 kV). Before imaging, samples were sputter-coated with a 5 nm gold layer to improve electron conductance.

#### 2.8. Statistic analysis

All significance analysis was done on triple duplicates unless specified.

#### 3. Results

#### 3.1. Fabrication of carbon micropillar array electrode

The fabricated SU-8 micropillar arrays on a silicon wafer were made conductive through a carbonization process following a common carbon MEMS procedure [50,51]. During this process, SU-8 micropillars experience complicated chemical processes, including oxidation, cyclization, dehydrogenation, aromatization, and crosslinking. Obviously, mass loss and dimension changes are unavoidable. When comparing the SEM images of SU-8 micropillars (Fig. 2b) and carbon micropillars (Fig. 2d), the structure and pattern of micropillar arrays are nicely retained, despite of some weight loss and size shrink occurrence. Both the height and diameter of the produced micropillars are shrunk ~50-60% of their original value after carbonization, with height changing from 1.5 μm to  $0.6 \mu m$  and micropillar diameter from 1.5  $\mu m$  to 0.7  $\mu m$ . As the consequence, the gap between micropillars changes from 2.2 µm to 3.0 µm. The shrunk micropillars allow more focused pulse strength on the micropillar far end and more localized disruption of the plasma membrane. The enlarged gap between micropillars, though reduces the density of porated spots on individual cells, improves the sag of their body among micropillar array to loosen the lipid layer packing status (Fig. 1b). Such structural changes are believed beneficial for effective electroporation [52].

#### 3.2. Enhancement of FME on reporter gene transfection

The FME electroporation was first tested on A549 cells and K562 cells for DNA plasmid delivery to demonstrate its effectiveness for both adherent and suspension mammalian cells. For comparison purpose, electroporation using both a commercial system (denoted as "BE") and batch-type micropillar array electroporation without flow (denoted as "BME") were also carried out in parallel. Successful transfection is observed in all three cases with many cells expressed green fluorescence protein (GFP) (Fig. 3a-d). Their quantitative difference on GFP-positive cells was further measured with an Agilent 2100 Bioanalyzer and a flow cytometer (CytoFLEX, Beckman Coulter). The results from these two systems were found similar (supp Fig. 1). As summarized in Fig. 3e & f and supp Fig. 2, the transfection efficiency with a FME device (76.2 ± 2.2% for K562 cells and 77.73  $\pm$  0.9% for A549 cells) and with a BME (70.3  $\pm$  2.5% for K562 cells and 71.3 ± 1.6% for A549 cells) device is much better than that from the commercial system (BE: K562: 25.7 ± 1.8%, A549: 22.0 ± 0.9%). To rule out potential auto-fluorescence interference caused by cell fragments, control samples (control II in which cell experienced the same electroporation treatment without plasmid addition) were also measured for comparison purpose. As shown in Supp Fig. 2, the auto-fluorescence caused by cell fragments in all events is less than ~10% (7.56% for BE and 5.28% for FME) and less than ~1.5% of the gated population (0.94% for BE and 1.23% for FME), which falls in the similar level like the other type of control samples (cell samples with plasmid added but no

electroporation treatment: ~6.20% for all events and ~0.75% for gated events). This suggests that auto-fluorescence contribution to the gated GFP signals from FME treated cell samples is ignorable. These results confirm the enhancement of FME on plasmid transfection to mammalian cells and such enhancement of FME and BME is about the same, attributed to their identical micropillar array feature on the electrode surface. As the micropillar electrode serves as the bottom surface of the flow slit, cells tend to migrate towards the micropillar surface by gravity naturally despite its flow-through operation, creating similar contact proximity as in its non-flow configuration (i.e., BME). The common loss on the cell viability (~10−15%) observed in the batch operation mode (BME) is not seen here in FME operation (Fig. 3e and f). Our previous suspect on hydrolysis-associated negative impact on cells in BME seems getting eliminated when a flow-through operation is adopted (see Section 3.7 for detailed discussions). Nevertheless, besides effective transfection, the cell viability of FME for both cell lines is above 80%, desirable for most biological and therapeutic application requirements.

#### 3.3. Enhancement of FME on other cell lines

To demonstrate the broad effectiveness of FME in plasmid DNA transfection improvement, more cell lines were tested. As shown in Fig. 4a and b, similar high transfection efficiency is observed in both common cell lines widely used in transfection tests  $(68.7 \pm 3.8\% \text{ for HeLa cells}, 75.2 \pm 0.9\% \text{ for COS7}, 92.3 \pm 2.3\% \text{ for COS7}$ 293T cells) and stem cells (50.2 ± 1.4%). As for comparison, the transfection results with BME and BE are also provided. These results confirm that the enhancement of FME on plasmid transfection is broadly effective to various mammalian cell lines including stem cells. Such enhancement level is equal for the flow-through type (i.e., FME) and the batch type operation ("BME"). As long as the same electrode configuration is used (i.e., with micropillar array pattern on electrode surface), the adoption of FME for highthroughput transfection does not introduce negative impact on plasmid delivery to cells. The cell viability varies with different cell types (76.5  $\pm$  8.4% for HeLa cells, 84.7  $\pm$  0.6% for COS7, 83.7  $\pm$  1.9% for 293 T cells, and 87.0 ± 1.9% for mES cells). Like our early observation in K562 cells and A549 cells, similar high cell viability is achieved for all four cell lines (Fig. 4c). The common loss on the cell viability in BME is not seen when adopting the flow-through operation (i.e., FME). It is worth to point out that all these transfection tests were done under the same electric pulse conditions (625 V/ cm, single pulse with a duration of 10 ms), which might not be best for some cell types. For example, COS-7 cells, which has exceptional high cell viability from COS7 cell samples). Suboptimal pulse conditions for some types of cells (e.g., COS-7) may allow more cells survive after electroporation. The 24-hour further culturing period before viability measurement might help their better recovery than other cell types to offset the hydrolysis associated negative impact imposed on these cells. Nevertheless, these results verify the excellent compliance of FME in different cell lines.

#### 3.4. Pulse focusing and Cell-Micropillar contact situations in FME

Like its batch-operation sibling system, the transfection improvement of FME is attributed to several advantages associated with the adoption of well-defined micropillar array electrode. The first one lies on the focusing of electric field on the far end of those carbon micropillars to cause local electroporation on the plasma membrane of cells nearby. In FME, the diameter of individual micropillars decides the overall pulse focusing level during electroporation while the pitch size between micropillars determines the pulse targeting spot number each cell faces and their separation distance between neighbor focusing spots on the cell membrane

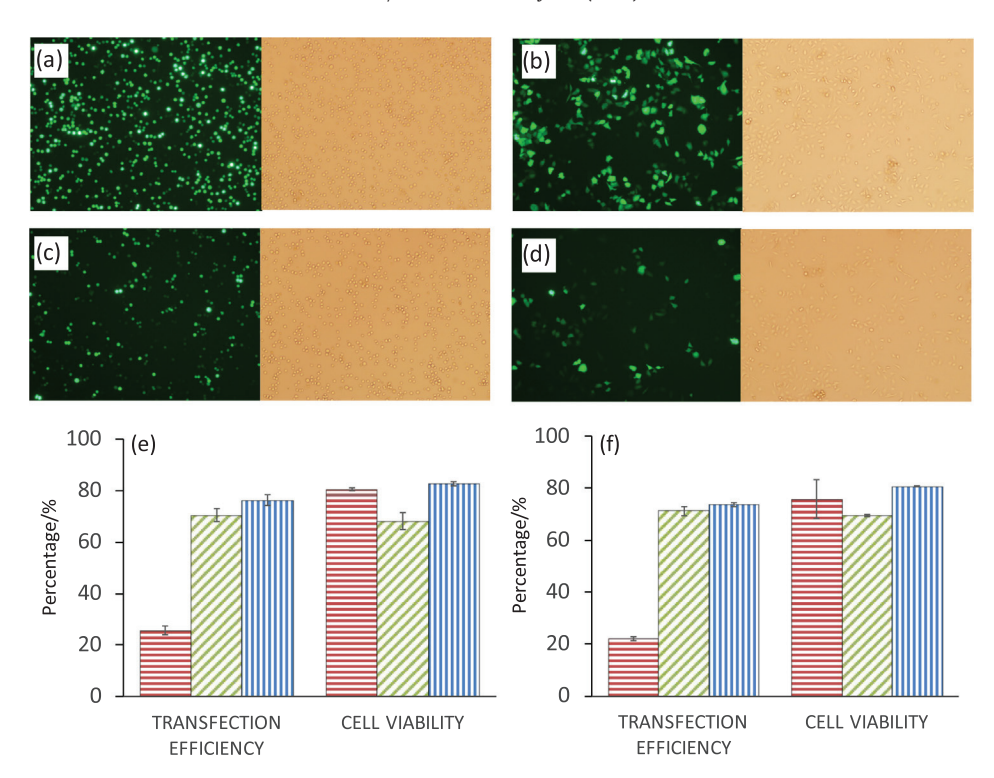


**Fig. 3.** Transfection enhancement of pGFP plasmids by 2-μm micropillar FME (flow-through operation of micropillar array electroporation). Phase contrast and fluorescence microscopic images of K562 cells (a, c) and A549 cells (b, d) with panels (a, b) for the transfection results of FME and panels (c, d) of a commercial cuvette-based batch operation system ("BE") for K562 and A549 cells, respectively. Panels (e) and (f) are the quantitative comparisons on the transfection efficiency and cell viability of FME (columns with blue, vertical stripes), BME (batch operation of micropillar-array electroporation, columns with green, upward diagonal stripes), and BE (columns with red, horizontal stripes) for K562 cells (e) and A549 cells (f), respectively.

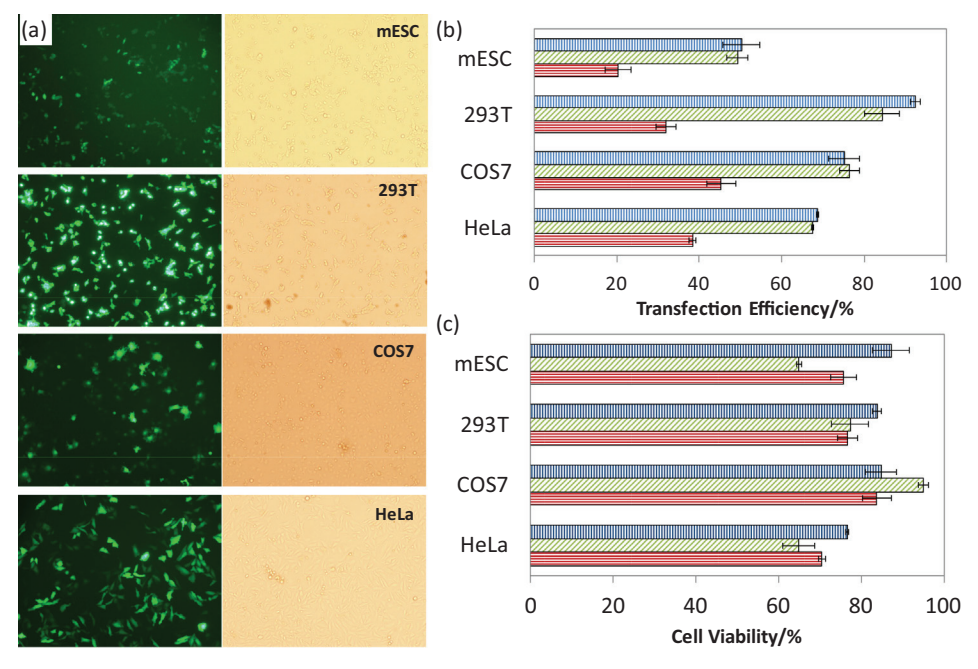


**Fig. 4.** Transfection performance of pGFP plasmids in other mammalian cell lines (HeLa, COS-7, 293T, and mES cells) with 2-μm micropillar FME (bars with blue, vertical stripes). Results from BME (bars with green, upward diagonal stripes) and BE (bars with red, horizontal stripes) are included for comparison.

(Fig. 1). Such enhancements are more effective when cells are in close proximity contact with micropillars. But unlike in BME platform where external pressure from two parallel electrodes squeezes the sandwiched cells solution towards micropillar top, cells in FME migrate towards the micropillar surface by gravity and normal forces during its flow-through operation (see Supp

movie in the supplemental materials for details). If similar cell-micropillar close contact situations still exist, the transfection enhancement effect in FME should also reflect some differences when the size and/or density of micropillars vary like what occurred in a BME platform. To verify such similarity on focusing effect in both batch and continuous flow operations, micropillars

of 6  $\mu m$  and 2  $\mu m$  in diameter with the same gap size of 2  $\mu m$  were tested in FME. As demonstrated in Fig. 5a and 5b, the transfection efficiency of 2-μm micropillar FME is ~76%, and 74% for K562 and A549 cells, respectively, while ~70%, and ~62% for those using 6um micropillars, and both were much higher than the one using parallel plain plate electrodes in cuvettes of BE. As smaller micropillars focus the local field strength to a higher level with the same applied electric potential, the focused pulses through carbon micropillars of 2  $\mu m$  are allocated more spots on the cell membrane. As the consequence, more but smaller porated individual openings are received for subjected cells to gain enhanced transfection efficiency. The dependence of transfection enhancement to the size of micropillars and the gap among them confirms the similar cell settlement on micropillar array surface when switching this micropillar array electroporation from batch to microfluidic mode.

#### 3.5. Transfection to broad cell size population in FME

With focused pulses and close contact of micropillars with cell membrane, FME should also be effective for cells of various size populations, despite their different sizes and location. According to the electroporation theory, the transmembrane potential (TMP) on cells is not only proportional to the strength and angle of the electric field imposed on cell membrane location, but also the size and electrical properties of the treated cells. In another word, large cells experience higher imposed TMP than small cells. When cells of various size populations are placed in a uniform electric field, only cells of appropriate size range receive reversible breakdown of their cell membrane for successful payload delivery. Other cells, either fail to generate large enough permeable area to allow probe uptake (for smaller cells) due to the insufficient TMP or receive severe damage on their plasma membrane to recover and survive because of their overdosed TMP during electroporation (for larger cells). In commercial electroporation systems ('BE"), their pulse conditions therefore work effectively only for cells of certain size populations (i.e., the dominated size populations) due to the lack of simple and effective tools to specify sizedependent treatment. In another word, their recommended electroporation protocols are generally identified by a compromise of efficient transfection and cell viability during the trial-and-error based optimization. This can be clearly seen from their flow cytometry result, as shown in Fig. 6a. The GFP positive cells (yellow dots) centralize in a limited range  $(1.2-2.8 \times 10^6)$  among all counted cells (black dots) for their forward scattered signal (FSC). As the forward scattered signal in flow cytometry generally reflects the size of cells, this result confirms that the commercial electroporation system works effectively on the medium size cells mainly, which in most cases, are also the ones with the largest populations in the cell samples. Different from the BE sample, the forward scattering signal from FME is much stronger and extends in both directions of their FSC signal, indicating its successful transfection to almost every size population of counted cells (Fig. 6b), despite of the large scattering of data. Their similar overall dot-plot patterns for SSC signals (Fig. 6a & b) as compared to the control samples shown in Supp Fig. 3a1 suggest that FME did not impose additional cell shape changes, affecting cell morphology like other electroporation systems.

#### 3.6. Carbon electrode effect

To avoid worn out issues for gold coated micropillar electrodes, total carbon micropillar electrode is adopted in FME instead. To examine their potential impact on cell transfection and viability, electrodes made of various materials commonly used in microelectroporation are integrated on similar microfluidic channels as in

FME. To rule out possible contributions from other than the closely placed configuration, plain parallel plate electrode of carbon, goldcoated SU-8 PR, and platinum without textured surface were tested in the same flow conditions. For comparison purpose, electroporation using commercial Al cuvettes also carried out in parallel as benchmark. As shown in Fig. 7, plain plate electrodes made of platinum, gold-coated and glassy-carbon receive a similar transfection level of ~50%, all much higher than what in the cuvette-based Al electrodes. The transfection efficiency improvement is mainly attributed to the closely placed configuration of electrode, which is consistent with our early findings [44]. No obvious sacrifice of cell viability was observed for flow-through electroporation with various electrode materials. This demonstrates that the glassy carbon electrode used in FME is equally effective as other electrode materials used in microelectroporation. But unlike those precious metal coated ones, the whole carbon electrodes used in FME are easier for fabrication, integration, and more durable in frequent pulse applications and flow involved operation.

#### 3.7. Contributions of microfluidics in FME

The introduction of microfluidics in FME contributes to the suppression of the electrohydrolysis and Joule heating issues that are widely observed in batch-type of electroporation treatment with still fluid [14–16]. The induced gas bubble evolution dynamics not only disrupts the local pulse field around cells, changes nearby pH value, but also causes severe damages to porated cells when they are in weak, permeable status. As the consequence, extra loss on cell viability is often observed. The adoption of a slit-type flow operation in FME largely mitigates such cell toxicity issues, confirmed by the 10-15% higher on cell viability for K562 and A549 cells when compared to its batch operation counterpart ("BME"), as shown in Fig. 3e and f. This improvement on cell viability could be attributed to two aspects: (1) continuous flow limits the number and size of gas bubbles associated with electrohydrolysis and Joule heating. The generated gas bubbles are quickly flushed away from the electrode surface by flow to prevent their growing so that no severe damage to surrounding cells. (2) quick dilution of treated cells into excessive culture medium to largely limit their exposure time to local pH variation near the micropillar electrode surface. These advantages allow FME to improve its transfection effectiveness without obvious compromise on cell viability, making it desirable for most biological and therapeutic application requirements.

Besides the cell survival benefit, flow operation also helps achieve high processing rate for FME. As for proof of concept and comparison purpose, single microfluidic slit is used in this work to process the same number of cells as in standard electroporation. Its current processing rate is around  $6 \times 10^7$  cells/hour (estimated based on 5  $\times$  10<sup>6</sup> cells per 240 s, plus 60 s extra time). Given its adoption on carbon electrode and slit type configuration using the electrode pair also as the channel wall, multiple FME units could be quickly stacked up or spirally wound into a large enough FME module to accomplish rapid transfection and high throughput processing of this size specific electroporation treatment. For example, with 20 FME units of the same size used in this work  $(L \times W \times H = 2.54 \text{ mm} \times 1 \text{ mm} \times 0.16 \text{ mm})$ , it could easily achieve a cell processing rate of 10<sup>9</sup> cells/hour. If further expanding the slit dimensions to 10 mm  $\times$  10 mm  $\times$  0.16 mm (L  $\times$  W  $\times$  H), the processing capacity of one FME module with 25 such FME units can handle 100 ml cell samples in 5 min (100 µl per 300 s  $\times$  40  $\times$  25), enough for most practical needs in drug screening, cancer immune therapy, or cell reprogramming applications on both cell population and processing time requirements.

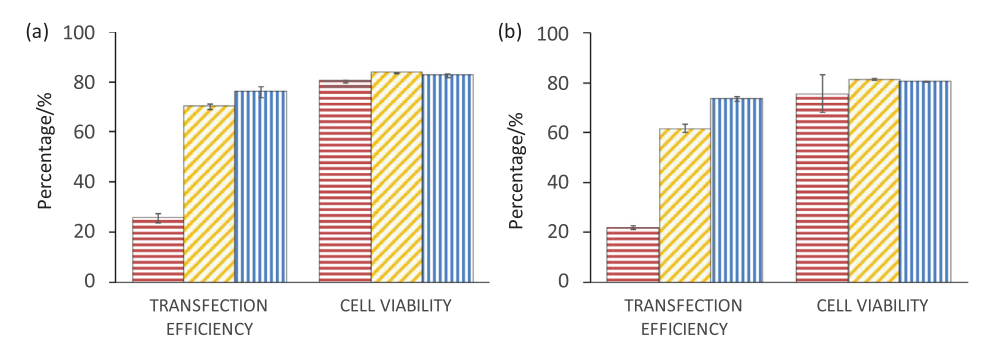


**Fig. 5.** The size effect of micropillars in FME on transfection enhancement: (a) K562 cells (b) A549 cells. Columns with blue, vertical stripes are results from 2-μm micropillar array electrode and columns with orange, upward diagonal stripes are from 6-μm micropillar array electrode. Results from BE (columns with red, horizontal stripes) are included for comparison.

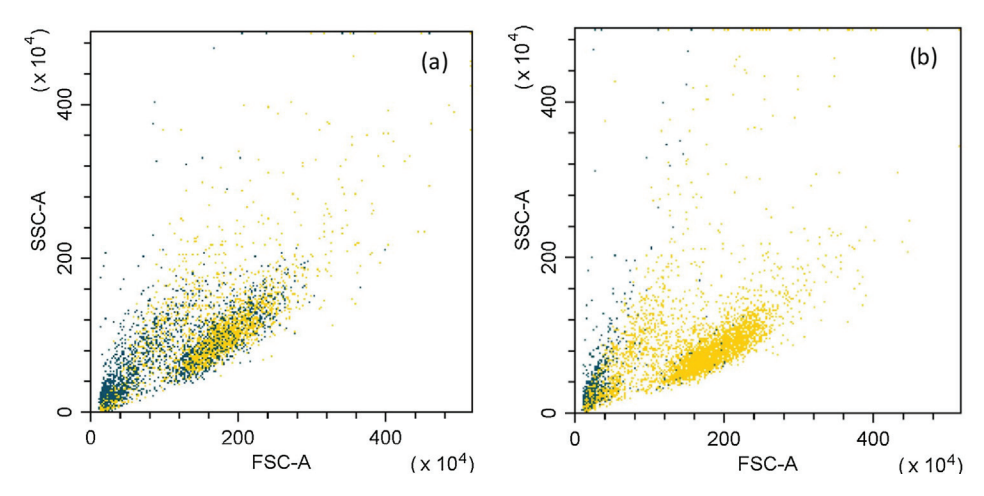


**Fig. 6.** The dot plots of flow cytometry results for GFP expression in various size populations of transfected K562 cells by (a) a commercial electroporation system ("BE") and (b) a 2-μm micropillar FME system. Dark green dots are for all events and yellow dots are for GFP positive events.

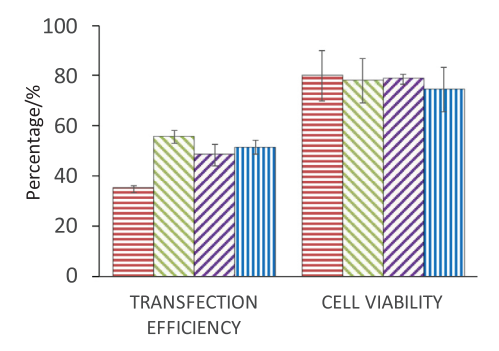


**Fig. 7.** GFP plasmids transfection performance in K562 cells using plain plate electrodes made of various materials (Carbon: columns with blue, vertical stripes; Au: columns with purple, upward diagonal stripes; Pt: columns with green downward diagonal stripes). Results from cuvette-based batch operation of BE with Al parallel plate electrodes is included for comparison (columns with red, horizontal stripes).

#### 4. Conclusion

To conclude, a new FME system is designed and demonstrated to enhance electroporation-mediated DNA delivery to both adherent and suspension cells of a large population with high throughput. Its well-defined micropillar array electrode configuration enables cell size specific treatment to many cells simultaneously regardless their size and random dispersion status. Its flow-through operation further allows many single cell electroporation

to work not only in parallel, but also in a continuous mode so that such size-dependent electroporation can be done to a large population of cells rapidly. Its success may benefit many emerging transfection explorations and clinical practice in drug screening, immune therapy, and cell reprogramming that requires rapid, effective transfection to a large population of cells within restricted processing time.

### **Declaration of Competing Interest**

The authors declare that they have no known competing financial interests or personal relationships that could have appeared to influence the work reported in this paper.

#### Acknowledgements

This work was supported by National Science Foundation Grant (1662735).

#### Appendix A. Supplementary material

Supplementary data to this article can be found online at https://doi.org/10.1016/j.bioelechem.2019.107417.

#### References

[1] J. Gehl, Electroporation: theory and methods, perspectives for drug delivery, gene therapy and research, Acta. Physiol. Scand. 177 (2003) 437–447.

- [2] D.C. Chang, D.C. Chang (Eds.), Guide to electroporation and electrofusion, Academic, 1992.
- [3] S. Li, Electroporation protocols: Preclinical and clinical gene medicine, Humana Press, 2014.
- [4] D. Luo, W.M. Saltzman, Synthetic DNA delivery systems, Nat. Biotechnol. 18 (2000) 33–37.
- [5] S. Cooper, N. Brockdorff, Genome-wide shRNA screening to identify factors mediating Gata6 repression in mouse embryonic stem cells, Development 140 (2013) 4110–4115.
- [6] D.H. Hamer, P. Leder, Splicing and the formation of stable RNA, Cell 18 (1979) 1299–1302.
- [7] J.L. Rae, R.A. Levis, Single cell electroporation, Eur. J. Physiol. 443 (2002) 664–670.
- [8] K. Nolkrantz, C. Farre, A. Brederlau, R.I.D. Karlsson, C. Brennan, P.S. Eriksson, S.G. Weber, M. Sandberg, O. Orwar, Electroporation of Single cells and tissues with an electrolyte-filled capillary, Anal. Chem. 73 (2001) 4469–4477.
- [9] J. Olofsson, K. Nolkrantz, F. Ryttsen, B.A. Lambie, S.G. Weber, O. Orwar, Singlecell electroporation, Curr. Opin. Biotechnol. 14 (2003) 29–34.
- [10] E.S. Yeung, Study of single cells by using capillary electrophoresis and native fluorescence detection, J. Chromatogr. A 830 (1999) 243–262.
- [11] E. Neumann, M. Schaefer-Ridder, Y. Wang, P.H. Hofschneider, Gene transfer into mouse lyoma cells by electroporation in high electric fields, EMBO. J. 1 (1982) 841–845.
- [12] E. Neumann, S. Kakorin, Radiol. Oncol. 32 (1998) 7.
- [13] K.K. Phua, D. Boczkowski, J. Dannull, S. Pruitt, K.W. Leong, S.K. Nair, Whole Blood Cells Loaded with Messenger RNA as an Anti-Tumor Vaccine, Adv. Health Mater. 3 (2014) 837–842.
- [14] S. Movahed, D. Li, Microfluidics cell electroporation, Microfluid. Nanofluid. 10 (2011) 703–734.
- [15] J.A. Kim, K. Cho, Y.S. Shi, N. Jung, C. Chung, J.K. Chang, A multi-channel electroporation microchip for gene transfection in mammalian cells, Biosens. Bioelectron. 22 (2007) 3273–3277.
- [16] S. Wang, X. Zhang, W. Wang, L.J. Lee, Semicontinuous flow electroporation chip for high-throughput transfection on mammalian cells, Anal. Chem. 81 (2009) 4414–4421.
- [17] Y. Huang, B. Rubinsky, Microfabricated electroporation chip for single cell membrane permiabilization, Sens. Actuators A 89 (2001) 242–249.
- [18] Y.C. Lin, C.M. Jen, M.Y. Huang, C.Y. Wu, X.Z. Lin, Electroporation microchips for continuous gene transfection, Sens. Actuators B 79 (2001) 137–143.
- [19] Y.S. Shin, K.J. Cho, K. Kim, S.H. Lim, C.H. Park, K.B. Lee, Y. Park, C. Chung, D. Han, J.K. Chang, Electroporation of mammalian cells using microchannel-type electroporation chip, Anal. Chem. 76 (2004) 7045–7052.
- [20] H. Lu, M.A. Schmidt, K.F. Jensen, A microfluidic electroporation device for cell lysis, Lab Chip 5 (2005) 23–29.
- [21] I. Obataya, C. Nakamura, S. Han, N. Nakamura, J. Miyake, Nanoscale operation of a living cell using an atomic force microscope with a nanoneedle, Nano Lett. 5 (2005) 27–30.
- [22] S.-W. Lee, Y.-C. Tai, A micro cell lysis device, Sens. Actuators A 73 (1999) 74–79.
- [23] E.G. Guignet, T. Meyer, Suspended-drop electroporation for high-throughput delivery of biomolecules into cells, Nat, Methods 5 (2008) 393–395.
- [24] O. Kurosawa, H. Oana, S. Matsuoka, A. Noma, H. Kótera, M. Washizu, Electroporation through a micro-fabricated orifice and its application to the measurement of cell response to external stimuli, Meas. Sci. Technol. 17 (2006) 3127–3133.
- [25] M. Khine, A. Lau, C. Ionescu-Zanetti, J. Seo, L.P. Lee, A Single cell electroporation chip, Lab. Chip. 5 (2005) 38–43.
- [26] N. Bhattacharjee, L.F. Horowitz, A. Folch, Continuous-flow multi-pulse electroporation at low DC voltages by microfluidic flipping of the voltage space topology, Appl. Phys. Lett. 109 (2016) 163702/1-5.
- [27] S. Wang, L.J. Lee, Biomicrofluidics 7 (2013) 011301.
- [28] P. Garcia, Z. Ge, J.L. Moran, C.R. Buie, Microfluidic screening of electric fields for electroporation, Sci. Rep. 6 (2016) 21238/1-11.
- [29] P.E. Boukany, A. Morss, W.C. Liao, B. Henslee, H. Jung, X. Zhang, B. Yu, X. Wang, Y. Wu, L. Li, K. Gao, X. Hu, X. Zhao, O. Hemminger, W. Lu, G.P. Lafyatis, L.J. Lee, Nanoelectroporation delivers precise amount of biomolecules into living cells, Nat. Nanotech. 6 (2011) 747–754.

- [30] J.A. Kim, K. Cho, M.S. Shi, W.G. Lee, N. Jung, C. Chung, J.K. Chang, A novel electroporation method using a capillary and wire-type electrode, Biosens. Bioelectron. 23 (2008) 1353–1360.
- [31] S. Wang, X. Zhang, B. Yu, R. Lee, L.J. Lee, Targeted nanoparticles enhanced flow electroporation of antisense oligonucleotides in leukemia cells, Biosens. Bioelectron. 26 (2010) 778–783.
- [32] H. Wang, C. Lu, Electroporation of mammalian cells in a microfluidic channel with geometric variation, Anal. Chem. 78 (2006) 5158–5164.
- [33] Z. Fei, S. Wang, Y. Xie, B. Henslee, C. Koh, L.J. Lee, Transfection of mammalian cells using membrane sandwich electroporation, Anal. Chem. 79 (2007) 5719–5722.
- [34] Z. Fei, X. Hu, H. Choi, S. Wang, D. Farson, L.J. Lee, Micronozzle array enhanced sandwich electroporation of embryonic stem cells, Anal. Chem. 82 (2010) 353– 358
- [35] Z.W. Wei, D. Zhao, X. Li, M. Wu, W. Wang, H. Huang, X. Wang, Q. Du, Z. Liang, Z. Li, A Laminar Flow electroporation system for efficient DNA and siRNA delivery, Anal. Chem. 83 (2011) 5881–5887.
- [36] T. Zhu, C. Luo, J. Huang, C. Xiong, Q. Ouyang, J. Fang, Electroporation based on hydrodynamic focusing of microfluidics with low dc voltage, Biomed. Microdevices 12 (2010) 35–40.
- [37] M. Wu, D. Zhao, W. Zhang, H. Yan, X. Wang, Z. Liang, Z. Li, High-density distributed electrode network, a multi-functional electroporation method for delivery of molecules of different sizes, Sci. Rep. 3 (2013) 3370/1-7.
- [38] D.A. Stewart, T.R. Gowrishankar, K.C. Smith, J.C. Weaver, Cylindrical cell membranes in uniform applied electric fields: validation of a transport lattice method, IEEE Trans. Biomed. Eng. 52 (2005) 1643–1653.
- [39] L. Chang, D. Gallego-Perez, C. Chiang, P. Bertani, T. Kuang, Y. Sheng, F. Chen, Z. Chen, J. Shi, H. Yang, X. Huang, V. Malkoc, W. Lu, L.J. Lee, Controllable Large-scale Transfection of Primary Mammalian Cardiomyocytes on a Nanochannel Array Platform, Small 12 (2016) 5971–5980.
- [40] D. Gallego-Perez, S. Ghatak, V. Malkoc, N. Higuita-Castro, S. Gnyawali, L. Chang, W. Liao, J. Shi, M. Sinha, K. Singh, E. Steen, A. Sunyecz, R. Stewart, J. Moore, T. Ziebro, R.G. Northcutt, M. Homsy, P. Bertani, W. Lu, S. Roy, S. Khanna, C. Rink, V.B. Sundaresan, J.J. Otero, L.J. Lee, C.K. Sen, Topical tissue nano-transfection mediates non-viral stroma reprogramming and rescue, Nat. Nanotech. 12 (2017) 974–979.
- [41] M. Golzio, J. Teissié, M.P. Rols, Direct visualization at the single-cell level of electrically mediated gene delivery, PNAS 99 (2002) 1292–1297.
- [42] M. Khine, C.I. Zanetti, A. Blatz, L.P. Wang, L.P. Lee, Single-cell electroporation arrays with real-time monitoring and feedback control, Lab. Chip. 7 (2007) 457-462
- [43] A. Valero, J.N. Post, J.W. van Nieuwkasteele, P.M. ter Braak, W. Krujier, A. van den Berg, Gene transfer and protein dynamics in stem cells using single cell electroporation in a microfluidic device, Lab. Chip. 8 (2008) 62–67.
- [44] Y. Zu, S. Huang, Y. Lu, X. Liu, S. Wang, Size specific transfection to mammalian cells by micropillar array electroporation, Sci. Rep. 6 (2016) 38661/1-10.
- [45] Y. Wu, M. Crawford, B. Yu, Y. Mao, S.P. Nana-Sinkam, L.J. Lee, MicroRNA delivery by cationic lipoplexes for lung cancer therapy, Mol. Pharm. 8 (2011) 1381-1389.
- [46] A.F. Adler, C.L. Grigsby, K. Kulangara, H. Wang, R. Yasuda, K.W. Leong, Nonviral direct conversion of primary mouse embryonic fibroblasts to neuronal cells, Mol. Ther. Nucleic Acids. 1 (2012) e32.
- [47] K.K. Phuaa, S.K. Nair, K.W. Leong, Messenger RNA (mRNA) nanoparticle tumor vaccination, Nanoscale 6 (2014) 7715–7729.
- [48] K. Takahashi, S. Yamanaka, Induction of pluripotent stem cells from mouse embryonic and adult fibroblast cultures by defined factors, Cell 126 (2006) 663–676.
- [49] Y.H. Kim, S.G. Kwon, S.J. Bae, S.J. Park, D.J. Im, Optimization of the droplet electroporation method for wild type Chlamydomonas reinhardtii transformation, Bioelectrochemistry 126 (2019) 29–37.
- [50] C. Wang, G. Jia, L.H. Taherabadi, M.J. Madou, A novel method for the fabrication of high-aspect ratio C-MEMS structures, J. Microelectromech. Syst. 14 (2005) 348–358.
- [51] J. Chen, Y. Zu, K. Rajagopalan, S. Wang, Flow-guided manufacturing of nanowire-based sensing system with microchannel template, Nanotechnology 26 (2015) 235603/1-8.
- [52] Q. Zheng, D.C. Chang, High efficiency transfection by in situ electroporation of cultured cells, Biochim. Biophys. Acta (Gene Struct. Exp.) 1088 (1991) 104–110.